

# Local observation and prediction of plastic rearrangements in a flowing foam

P. Marmottant, B. Dollet,\* C. Raufaste, and F. Graner

*Laboratoire de Spectrométrie Physique, B.P. 87, F-38402 St Martin d'Hères Cedex, France*<sup>†</sup>

The plastic flow of a foam results from localized bubble rearrangements. We study their occurrence in an experiment where a foam is forced to flow in 2D around an obstacle. We describe their orientation and frequency using a topological tensor which links them with macroscopic plasticity. We observe that they are aligned with the elastic deformation. We then suggest a phenomenological equation to predict the plastic strain rate from the foam's current elastic deformation and elongation rate. We obtain a good agreement with observations. This helps describing the foam as a continuous medium with fluid, elastic and plastic properties.

A liquid foam is elastic for small deformation, plastic for large deformation, and flows at large deformation rates [1, 2]. This complex mechanical behaviour is exploited in numerous applications, such as ore separation, drilling and extraction of oil, food or cosmetic industry [1], but is not yet fully understood [3].

Existing models of complex fluids include Oldroyd's visco-elasticity or Bingham's visco-plasticity [4, 5]. However, complete models which might unify elastic, plastic and fluid behaviour [6] still lack a microscopic basis.

A crucial step would consist in predicting the occurrence and properties of the microscopic plastic events [7], which in foams are the bubble rearrangements (neighbour swapping, also called "T1 processes" [1]). Does one necessarily require a detailed microscopic understanding of velocity fluctuations and T1 correlations [8]? Else, is a continuous description based on coarse-grained quantities sufficient? For instance, recent quasistatic simulations relate the T1s' orientations with the local stress [9]. Here, we attempt to completely characterize the T1s, and predict them from the foam's current elastic deformation and velocity gradient.

For that purpose, we perform an experiment in which a one-bubble-thick foam flows quasistatically around an obstacle [10]. The microscale is the scale of the bubbles, which act as convenient tracers of elastic deformation, rearrangements and velocity. Inspired by our observations, we suggest an analytical prediction of the T1s' orientation and frequency, based on the foam's elastic deformation and elongation rate. The relationship between experimental data agrees with our analytical prediction. Moreover, we correctly predict the spatial distribution of T1s, although it differs much from the spatial variations of both deformation and elongation rate.

The foam channel [10] is a 1 m long, 10 cm wide tank full of water with 1% commercial dishwashing liquid. We leave a 3.5 mm thick layer of air between the surface of water and a transparent horizontal glass plate. A computer-controlled flow of nitrogen through the water produces bubbles which fill this empty space. It yields

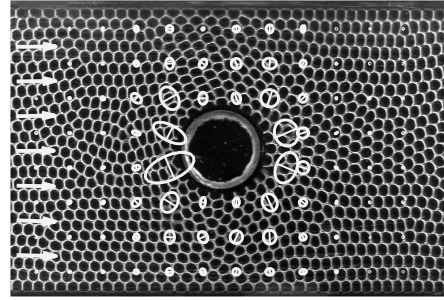


Figure 1: Fluid behaviour. Snapshot of the experiment: 2D flow, from left to right, of a foam around a circular obstacle. Superimposed "coffee bean" ellipses: measurements of the elongation rate tensor  $(\bar{G} + \bar{G}^t)/2$ ; ellipse axes are proportional to the eigenvalues, the line indicating the positive one (direction of elongation).

a disordered monolayer of monodisperse bubbles (area  $A_{bubble} = 16.0 \text{ mm}^2$ , fluid fraction  $\approx 7 \pm 1\%$ ) which reaches the free exit at the end of the channel. The resulting steady plug flow, at  $0.84 \text{ cm/s}$ , is well in the quasistatic regime [10]; it is bidimensional, i.e. without vertical velocity component. Coalescence and ageing are below detection level. We insert a circular obstacle which imposes a heterogeneous velocity field [10] (Fig. 1). Thus different regions simultaneously display different velocity gradients, elastic strains, and rearrangement rates.

In what follows,  $\langle \cdot \rangle$  denotes the average over a spatial box of area  $A_{box}$  and over a time  $\tau$ , that is over several movie images;  $N_{links} = 3\tau A_{box}/A_{bubble}$  is the number of links [1] in  $(A_{box}, \tau)$ . All figures are prepared with  $A_{box} = 37 \text{ mm}^2$  and  $\tau = 750$  successive video images. These values are large enough to coarse grain the information ( $N_{links} \gg 1$ ), and small enough to accurately describe spatial variations [11]. We checked that these choices do not affect the equations presented below.

\*Present address: Department of Science and Technology, University of Twente, P.O. Box 217, 7500 AE Enschede, The Netherlands.

<sup>†</sup>UMR5588, CNRS-Université Grenoble I

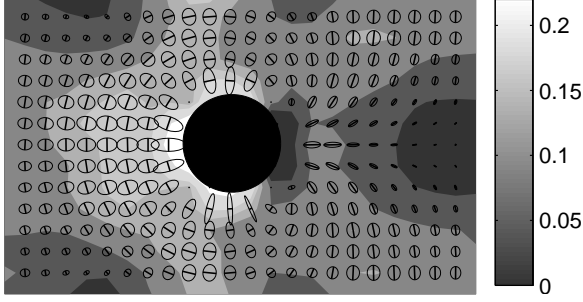


Figure 2: Elastic behaviour: map of the measurements of the foam's elastic strain. Coffee beans: tensor  $\bar{U}$  itself; ellipse axes indicate the direction and amplitude of stretching (indicated by a line) and compression. Grey levels: amplitude of its deviatoric term  $U_d = \|\bar{U}_d\|$ .

Image analysis yields the vector  $\vec{\ell}$  linking each pair of neighbouring bubble centers. The tensorial product of  $\vec{\ell}$  by itself, denoted by  $\vec{\ell} \otimes \vec{\ell}$ , is the rank two tensor of components  $\ell_i \ell_j$ , insensitive to the sign of  $\vec{\ell}$ . We thus measure the texture tensor  $\bar{M}$ , defined as in ref. [12], but here based on bubble centers:

$$\bar{M} \equiv \langle \vec{\ell} \otimes \vec{\ell} \rangle = \frac{1}{N_{\text{links}}} \sum_{(A_{\text{box}}, \tau)} \vec{\ell} \otimes \vec{\ell}. \quad (1)$$

Its eigenvalue  $\ell_+^2/2$  (resp.  $\ell_-^2/2$ ) reflects the average distance between bubbles in the elongated (resp. compressed) direction. The actual value, the time derivative and the discontinuities of  $\bar{M}$  characterise the foam's elastic, fluid and plastic behaviours, respectively. These tensors are measured statistically as follows.

*Elasticity.* The elastic strain  $\bar{U}$  is defined by comparing  $\bar{M}$  with its value  $\bar{M}_0$  in an undeformed state [12]:

$$\bar{U} \equiv \frac{1}{2} [\ln \bar{M} - \ln \bar{M}_0]. \quad (2)$$

This dimensionless tensor characterises the material's current deformation: relative dilation, amplitude and direction of anisotropy. If the foam is in the elastic regime, that is, if it is possible to follow individual displacements of microscopic components (here the bubbles), then  $\bar{U}$  coincides with the elastic strain defined from the gradient of the displacement field  $\vec{u}$ . This is the case even at large elastic deformations [13], where  $\bar{U}$  generalizes the uniaxial "true" strain [14]. In the limit of small deformations [12],  $\bar{U} \simeq \frac{1}{2}(\bar{M} - \bar{M}_0)\bar{M}_0^{-1}$  coincides with  $\bar{\varepsilon} = \frac{1}{2} [\vec{\nabla} \otimes \vec{u} + (\vec{\nabla} \otimes \vec{u})^t]$ . In the present experiment the elastic deformation remains small because plasticity occurs: the total strain is decomposed in elastic and plastic deformations  $\bar{\varepsilon} = \bar{\varepsilon}^e + \bar{\varepsilon}^p$  [14], and  $\bar{U}$  measures  $\bar{\varepsilon}^e$  [12].

The deviatoric elastic strain (shear, without dilation) is the traceless tensor  $\bar{U}_d = \bar{U} - (\text{Tr} \bar{U}) \bar{I}/2$ . Its amplitude is defined as  $U_d \equiv [(1/2) \sum_{i,j} (U_{d,ij})^2]^{1/2}$ . Physically,  $U_d$

measures the relative increase (resp. decrease) of bubble distances along the elongation (resp. contraction) eigenvector of  $\bar{U}_d$ . Up to a prefactor, namely the foam's shear modulus,  $(U_d)^2$  is the elastic energy stored (with respect to local minima) due to shear.

Fig. (2) shows that deformation is large in the whole region before the obstacle. Just before the obstacle, it reaches its maximum, which is  $U_d \simeq 0.2$ . This is a reasonable value for the yield strain of a foam with a fluid fraction slightly lower than the critical value of 9.1% (corresponding to the rigidity loss transition for a honeycomb) [15]. The foam is compressible (in this particular set-up [10]): else eigenvalues of the deformation would be opposite and equal in absolute value, meaning circular coffee beans on the figure.

*Fluidity.* We now define the deformation rate  $\bar{G}$ , as:

$$\bar{G} \equiv \langle \dot{\vec{\ell}} \otimes \vec{\ell} \rangle \bar{M}^{-1}. \quad (3)$$

It has the dimension of a shear rate ( $\text{s}^{-1}$ ), and quantifies at which rate vectors inside the considered box vary; in fact,  $\bar{G}\bar{M}$  appears in the time derivative of definition (1). If the velocity field  $\vec{v}$  is close to affine, that is if  $\dot{\vec{\ell}} \approx (\vec{\nabla} \otimes \vec{v})^t \vec{\ell}$ , then  $\bar{G} \approx (\vec{\nabla} \otimes \vec{v})^t$ . Thus  $\bar{G}$  appears as a statistical measurement, which does not require any spatial derivation, of the transposed velocity gradient  $(\vec{\nabla} \otimes \vec{v})^t$ .

Fig. (1) plots its symmetrical part, the elongation rate  $(\bar{G} + \bar{G}^t)/2$ . It is large all around the obstacle, but only very close to it; it is almost symmetrical before and after the obstacle.

*Plasticity.* T1s involve four bubbles (Fig. 3a). Two neighbour bubbles separate, the link  $\vec{\ell}_d$  between their centers disappears. Then a new link  $\vec{\ell}_a$  appears between two bubbles which come into contact. The texture thus undergoes a discontinuous variation  $\delta \bar{M} \equiv \vec{\ell}_a \otimes \vec{\ell}_a - \vec{\ell}_d \otimes \vec{\ell}_d$ . It implies a strain change of  $\delta \bar{U} = \delta \bar{M} \bar{M}^{-1}/2$ , from the differentiation of def. (2). Averaging over all discontinuities, we define another new topological tensor  $\bar{P}$  as:

$$\bar{P} \equiv -f \delta \bar{U} = f [\langle \vec{\ell}_d \otimes \vec{\ell}_d \rangle - \langle \vec{\ell}_a \otimes \vec{\ell}_a \rangle] \bar{M}^{-1}/2, \quad (4)$$

where  $f$  is the T1 rate per unit time and per link:  $f^{-1}$  is the average link's life expectancy. The tensor  $\bar{P}$  has the dimension of  $\text{s}^{-1}$  and measures the frequency, amplitude, and direction of rearrangements. When a rearrangement occurs, the elastic strain decreases by  $\delta \bar{\varepsilon}^e = \delta \bar{U}$  and the plastic strain increases by  $\delta \bar{\varepsilon}^p = -\delta \bar{U}$ . The plastic flow is therefore written  $d\bar{\varepsilon}^p/dt = -f \delta \bar{U} = \bar{P}$ .

Disappearing and appearing links seem to be determined in average by the existing deformation (Fig. 3b). The tensor  $\bar{P}$  makes an angle of  $0 \pm 9^\circ$  with  $\bar{M}$  or  $\bar{U}$ : disappearing links  $\vec{\ell}_d$  are mainly in the elongation direction. Their length is  $1.2 \pm 0.1$  times larger than the average of existing links in that direction. Conversely, links appear

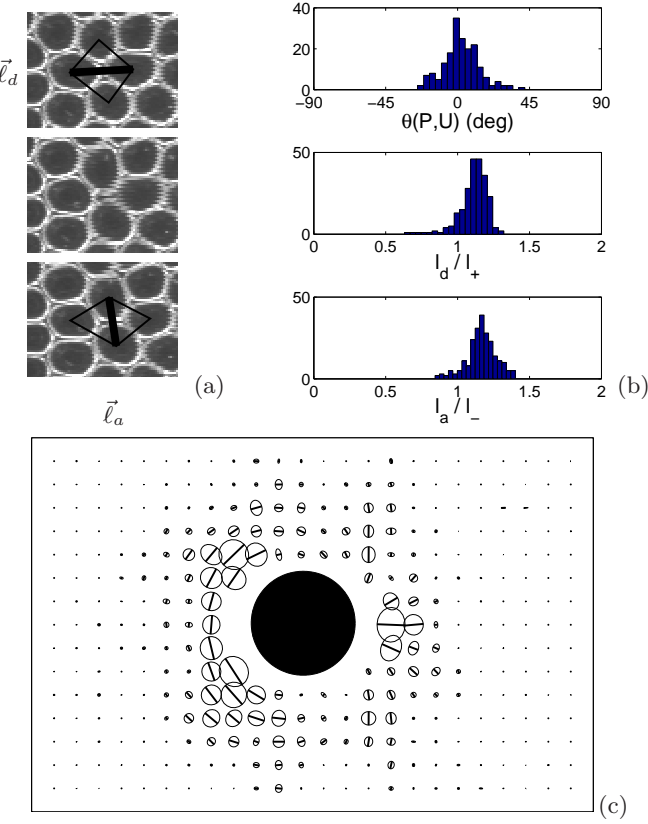


Figure 3: Plastic behaviour. (a) Topological rearrangement leading to plasticity: the vector  $\vec{l}_d$  linking two neighbouring bubble centers (thick line superimposed on left photograph) disappears between times 0 (top) and 40 ms (middle); then before time 120 ms (bottom) a new one  $\vec{l}_a$  appears (thickline). (b) Histograms of measurements in all regions of the foam. Top: angle between topological events and elongation. Middle: length of disappearing links compared to average length in elongation direction  $\ell_+$ . Bottom: length of appearing links compared to average length in compressed direction  $\ell_-$ . (c) Coffee beans: experimental measurements of the topological tensor  $\bar{P}$  defined in eq. (4). Here, the positive (resp. negative) eigenvalue, marked by a line (resp. no line) is the direction of links which have just disappeared (resp. just appeared). The size of ellipses is proportional to the frequency. Measurement boxes touching the obstacle were removed.

in the contracted direction of  $\bar{M}$ , with a length  $1.1 \pm 0.1$  times the average of existing links.

Fig. (3c) shows that the rearrangements are more frequent just in front of the obstacle, or in a very narrow region behind it. The rate of rearrangements decreases smoothly with the distance to the obstacle. This is due to the foam's elasticity. It contrasts with the sharp transition between solid-like and fluid-like regions observed in purely visco-plastic materials [16, 17].

*Model.* All above measurements suggest that the foam behaves as a continuous medium which could be described by partial differential equations. Elastic, plastic and fluid behaviours are characterised by quantities

$(\bar{U}, \bar{P}, \bar{G})$  which have smooth spatial variations. These quantities are not independent. In a pure elastic regime, the elongation rate is equal to the time derivative of the elastic strain. Conversely, they differ where the topological tensor  $\bar{P}$  does not vanish. A set of constitutive equations would thus require a closure equation, relating  $\bar{P}$  to the other variables. We thus now try to write a mean-field prediction, determining  $\bar{P} = \bar{P}(\bar{U}, \bar{G})$ .

Inspired by the observations (Fig. 3b), we first postulate that that each rearrangement changes the elastic strain by a constant amount:

$$\delta\bar{U} \approx -\hat{U}, \quad (5)$$

where  $\hat{U} = \bar{U}_d/U_d$  is the tensor that writes  $\text{diag}(1, -1)$  in the eigenvector basis of elongation. It is a mean field value assumption: strain is decreased by one average length in the elongation direction, and increased by one average length in the orthogonal direction.

Second, we postulate that the rate of rearrangements is fixed by the elongation rate according to:

$$f_Y \approx \max \left( 0, \frac{1}{4} \hat{U} : (\bar{G} + \bar{G}^t) \right). \quad (6)$$

It depends on the relative angle  $\theta$  between the elongation rate and deformation, expressed by the scalar product between tensors,  $\bar{A} : \bar{B} \equiv \sum_{i,j} A_{ij} B_{ij}$ . More precisely, it results in  $f_Y \approx \cos(2\theta)\dot{\varepsilon}$  when positive, where  $\dot{\varepsilon}$  is the positive eigenvalue of the elongation rate. This extends findings by [9]. It expresses that rearrangements are frequent where the deformation is strong, and when the elongation is parallel to the pre-existing deformation thus loading it through the yield surface. The frequency is such that the loading rate of the norm of deformation  $dU_d/dt = \hat{U} : (d\bar{U}/dt)/2$  is exactly balanced by the topological relaxation rate  $f\delta(U_d) = f\hat{U} : \delta\bar{U}/2 \approx f$  according to eq. (5). In the opposite case, if the elongation is in the direction opposed to deformation, and thus contributes to unload it elastically, it does not induce rearrangements; this is expressed by the “max” term, which tests the sign of the scalar product.

Injecting hyp. (5) and (6) in def. (4), the topological tensor near or just below the yield strain can be predicted to be:

$$\bar{P}_Y \approx \max \left( 0, \frac{1}{4} \hat{U} : (\bar{G} + \bar{G}^t) \right) \hat{U}. \quad (7)$$

Since  $\bar{U}$  relates to the microscopic origin of the macroscopic elastic stress, and specifies the amplitude of the relaxation, our postulate (eq. 7) provides a basis to the classical assumption used in the plasticity of polycrystalline metals, where rearrangements are oriented by elastic stress [14, 18]. We thus generalize to arbitrary deformations the plastic description for the uniform shear of a foam between two plates [8]. Here the influence of a rearrangement on the network,  $\delta\bar{U}_d$ , is explicitly formulated and we obtain a quantitative prediction.

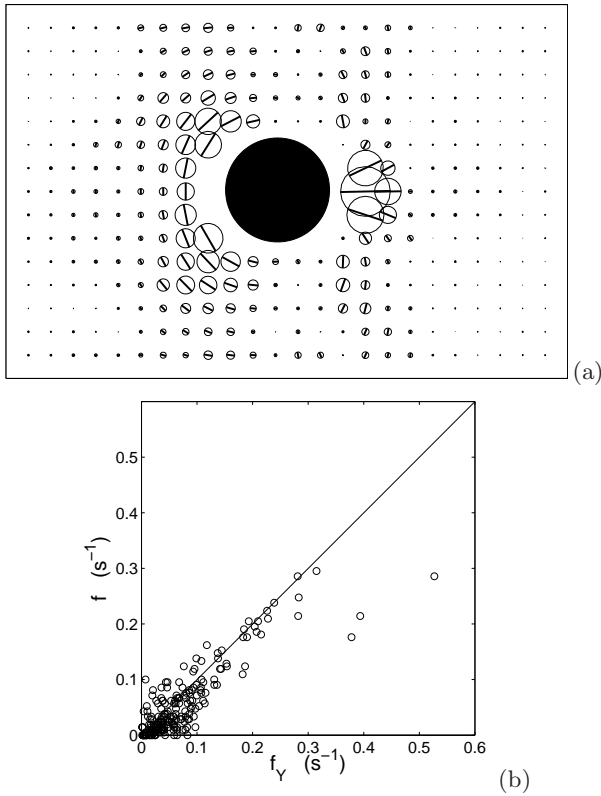


Figure 4: Tests of predictions from eq. (7), using data of Figs. (1) and (2). (a) Predicted map: compare with actual measurements of Fig. (3b). (b) Rearrangement frequency per link: observed  $f$  versus predicted  $f_Y = \hat{U} : (\bar{G} + \bar{G}^t)/4$ , set to zero where the scalar product is negative (far beyond the obstacle). Each point corresponds to one region of the foam, that is, one ellipse of the map (a). Solid line:  $f = f_Y$ .

Hyp. (7) is derived from quasistatic observations near or just below the yield strain, which is where most rearrangements occur; it is thus not necessarily valid at much lower elastic strain or at much higher flow rate. Note that it is purely geometrical and thus does not involve the stress, the energy, nor the elastic modulus.

Since we have measured all terms in hyp. (7), we

can quantitatively test its prediction. The predicted  $\bar{P}_Y$  agrees very well with the observed  $\bar{P}$ , without adjustable parameter (Fig. 4). The same experiment was performed with a very dry foam (water fraction 0.01 %) between two glass plates: it yielded a similarly good agreement between experiments and prediction (data not shown).

We predict well the spatial distribution of T1 events: they occur mostly just before the obstacle, and in a narrower region after it (Fig. 4a). We also predict well the direction of rearrangements, as well as their amplitude, represented by the direction of the coffee beans and their size, respectively.

Rearrangement frequency is well predicted almost everywhere (Fig. 4b). It is overestimated in the high shear region: this might be explained by compression effects [10] that we have not taken into account. It is also overestimated in regions of low shear, far from the obstacle, where advection (that we have not taken into account) dominates plastic relaxation.

The origin of the upstream/downstream asymmetry of plasticity can now be explained. The obstacle imposes a succession of symmetric opposite elongation rates: spanwise before the obstacle, and streamwise after it (Fig. 1). Before the obstacle, the elastic deformation (Fig. 2) and the elongation rate are aligned, and the foam is yielding (Fig. 3). After the obstacle, it takes some time until the bubbles fully relax, then deform again in the new direction of elongation, orthogonal to the initial one. Topological rearrangements are therefore concentrated in a smaller region. Because of the elastic nature of the foam, the plastic flow depends on the elongation rate and on the present amplitude of deformation.

The modelisation uses variables which are general enough to apply to elastic, plastic and fluid regimes. Since it is in tensorial form, it also applies in 3D. It should thus apply to a wide class of complex materials, which individual constituents subject to rearrangements could be atoms, molecules, bubbles, droplets or solid particles (the vector  $\vec{l}$  being in each case the link between neighbouring microscopic objects [12]).

---

[1] D. Weaire and S. Hutzler, *The physics of foams* (Oxford University Press, Oxford, 1999).  
[2] A. Saint-Jalmes and D. Durian, *J. Rheol.* **43**, 6 (1999).  
[3] R. Höhler and S. Cohen-Addad, *J. Phys. Cond. Matt.* **17**, R1041 (2005).  
[4] N. Phan-Thien, *Understanding viscoelasticity* (Springer-Verlag, Berlin, 2002).  
[5] C. W. Macosko, *Rheology : principles, measurements and applications* (Wiley-VCH, 1994).  
[6] E. Janiaud, D. Weaire, and S. Hutzler, *Phys. Rev. Lett.* **97**, 038302 (2006).  
[7] G. Picard, A. Ajdari, F. Lequeux, and L. Bocquet, *Eur. Phys. J. E* **15** (2004).  
[8] A. Kabla and G. Debrégeas, *Phys. Rev. Lett.* **90**, 258303 (2003).  
[9] S. Vincent-Bonnieu, R. Höhler, and S. Cohen-Addad, preprint.  
[10] B. Dollet, F. Elias, C. Quilliet, C. Raufaste, M. Aubouy, and F. Graner, *Phys. Rev. E* **71**, 031403 (2005).  
[11] I. Goldhirsch and C. Goldenberg, *Eur. Phys. J. E* **9**, 245 (2002).  
[12] M. Aubouy, Y. Jiang, J. A. Glazier, and F. Graner, *Granular Matt.* **5**, 67 (2003).  
[13] E. Janiaud and F. Graner, *J. Fluid Mech.* **532**, 243 (2005).  
[14] J. Chakrabarty, *Theory of plasticity* (McGraw-Hill Book

Company, New York, 1978).

[15] H. M. Princen, *J. Coll. Interf. Sci.* **91**, 160 (1983).

[16] A. N. Beris, J. A. Tsamopoulos, R. C. Armstrong, and R. A. Brown, *J. Fluid Mech.* **158**, 219 (1985).

[17] J. Blackery and E. Mitsoulis, *J. Non-Newt. Fluid Mech.* **70**, 59 (1997).

[18] B. de Saint-Venant, *C. R. Acad. Sci., Paris* **70**, 473 (1870).